

Real-Time Pulse Echo and Photoacoustic Imaging Using an Ultrasound Array and In-line Reflective Illumination

Leonardo G. Montilla*, Ragnar Olafsson, and Russell S. Witte
Department of Radiology, University of Arizona
Tucson, AZ USA

ABSTRACT

Recent clinical studies have demonstrated that photoacoustic (PA) imaging, in conjunction with pulse echo (PE) ultrasound is a promising modality for diagnosing breast cancer. However, existing devices are unwieldy and are hard to integrate into the clinical environment. In addition, it is difficult to illuminate thick samples because light must be directed around the transducer. Conventional PA imaging designs involve off-axis illumination or transillumination through the object. Whereas transillumination works best with thin objects, off-axis illumination may not uniformly illuminate the region of interest. To overcome these problems we have developed an attachment to an existing clinical linear array that can efficiently deliver light in line with the image plane. This photoacoustic enabling device (PED) exploits an optically transparent acoustic reflector to co-align the illumination with the acoustic waves, enabling real-time PA and PE imaging. Based on this concept, we describe results from three types of PEDs in phantoms and rat tissue. The most recent version is fabricated by rapid prototyping, and attached to a 10 MHz linear array. Real-time PA and PE images of a 127- μm diameter wire were consistent with our expectations based on the properties of the ultrasound transducer. Comparisons with and without the PED of another test phantom printed on transparency demonstrated that the PED does not appreciably degrade or distort image quality. The PED offers a simple and inexpensive solution towards a real-time dual-modality imaging system for breast cancer detection. It could also be adapted for virtually any kind of ultrasound transducer array and integrated into routine ultrasound exams for detection of cancerous lesions within 1-2 cm from the probe surface.

Keywords: Clinical ultrasound, mammography, breast cancer, optoacoustic, photoacoustic enabling device, reflection mode photoacoustics

1. INTRODUCTION

Breast cancer is the leading cause of malignancy-associated death among women in the world causing over 400,000 deaths in 2002¹. X ray mammography is the primary screening process for the screening of breast cancer while other imaging modalities such as ultrasonography and magnetic resonance offer second stage detection before a possible invasive biopsy. X-ray mammography, in addition to using hazardous ionizing radiation and patient discomfort, suffers from a high number of false-positives, a relatively low sensitivity and sometimes false-negatives especially in radiographically dense breast². Photoacoustic imaging (PAI) is an emerging ultrasound technology that can potentially enhance and complement current ultrasound screening, which has high sensitivity, but low specificity².

Early clinical studies have demonstrated the ability for PAI to detect malignant lesions^{3, 4}. The high contrast PA images of breast tumors takes advantage of the higher optical absorption in blood of the cancer microvasculature. These early studies illustrate cases where conventional mammography exhibited benign features, while the PA information correctly suggested malignancy. While X-ray mammography and ultrasonography each depict morphological information, PAI shows functional information directly correlated with cancer angiogenesis^{3, 4}. Furthermore, since ultrasound and PA images involve many technological similarities, their application in a dual modality system acquiring real-time information with complementary contrast mechanisms is practical and desirable⁵⁻⁷.

*Lgm@email.arizona.edu; phone 520 626-1936

However, significant challenges currently limit PA imaging from widespread clinical use. The geometrical constraint of the detector usually prevents direct illumination of the tissue, which becomes more difficult as the physical dimensions of the transducer increases, such as with an array of detector elements. To acquire quality images, the transducer should be acoustically coupled directly in front of the tissue while still illuminating the same region. Currently, various designs exist to redirect the light around a single element detector⁸⁻¹¹. However, these designs incorporate a setup involving custom parts, sensitive alignment, and a fragility difficult to apply in a clinical setting. Furthermore, these and similar designs have difficulty coupling sufficient light with the small illumination area available given the safety limits for laser exposure¹². In addition, most of these designs demand complicated deconvolution algorithms to make direct quantitative measurements possible¹². Conventional mammography and early clinical PA studies often compress the breast between two plates to allow for transillumination. Although this method succeeds in decreasing the imaging depth and ensures adequate coupling between the breast and the detector, patients suffer from physical discomfort during examinations and would welcome an alternative method. In-line reflection-mode illumination is preferred over transillumination because stronger signals are present near the transducer and because detectors have been shown to exhibit lower thermal background noise⁷. Another limitation to implementing PA imaging in the clinic is its current lack of portability. Most designs use a bulky laser that cannot be easily transported. In addition, designing a PA scanner would require redesigning current ultrasound transducers and building custom detector arrays as previous clinical setups have done^{13, 14}. The combination of all these challenges currently hinders PA technology from transitioning to clinical acceptance. To overcome some of the limitations, we describe a robust, inexpensive and portable PED that attaches to existing clinical ultrasound probes and offers in-line reflection-mode illumination.

2. MATERIALS AND METHODS

2.1 Concept Overview

A diagram illustrating the complete concept of the PED is shown in Figure 1. This design is based on work others have published using single element transducers^{11, 15}. The PED attaches to a clinical ultrasound probe enabling the simultaneous real time acquisition of PA data using in-line illumination¹⁶. The solid device can be thought of in three distinct parts – the probe mount, the reflector chamber, and the illumination block. The probe mount holds the clinical ultrasound array in place, the reflector chamber consists of the glass reflector and water and the illumination block contains the laser source, coupling optics, multimode fiber, fiber collimator and cylindrical lens. These parts can be designed in a single complete structure or can be made to be physically separable, creating a modular system for the integration of future components. A critical design element of the PED was the choice of the optically transparent acoustic reflector.

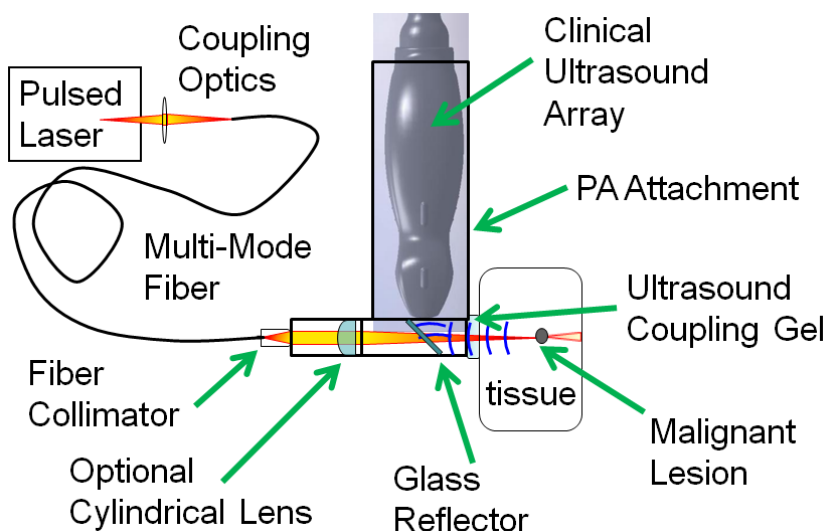


Figure 1. An overview of the system concept showing the ultrasound scanner, acoustic reflecting chamber, and the illuminating source packaged as a single attachment to enable PAI. The actual setup for this paper used free space optical illumination as shown in Figure 5.

2.2 Reflector Experiments

The ideal acoustic reflector for our design should not affect the illumination in any way. However, refraction on the boundaries between materials is a practical limitation. While it is possible to overcome these limitations by using an index matching liquid for acoustic transmission¹¹ we wanted to use water, as it is economical and easy to implement. To select an optically transparent acoustic reflector, we conducted some preliminary proof-of-concept experiments using available right angle prisms submerged in water. One implementation used a 25 mm right angle prism, below (Figure 2a). However, this reflector complicates optical alignment by chromatic diffraction. In an attempt to position the transducer closer to the prism and reduce the distance between the detector and object, a second design consisting of four 6 mm by 16 mm prisms bonded together was also constructed (Figure 2b). This parallel plane approach provides achromatic transmission, free from any optical deviation and dispersion. Extending the idea of a parallel plane to smaller thicknesses reduced the optical displacement due to refraction. Our first attempt to improve the reflector was the use of a 150- μ m thick cover slip. This reflector was quickly determined to be inadequate for our intention since we observed the transmission of acoustic waves through the glass in real-time PE imaging mode. However, similar real-time PE imaging experiments with a 1.0 mm thick microscope slide demonstrated that signals beyond the incident surface could not be detected and therefore the slide suggests a good reflector.

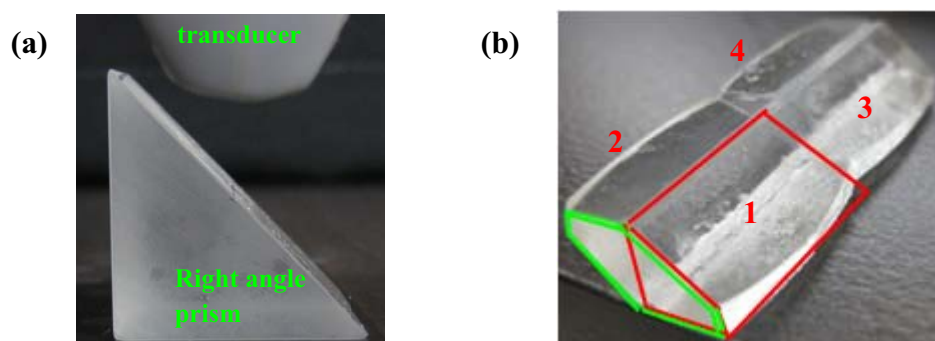


Figure 2. Two acoustic reflector designs set directly below a linear array detector, allowing light to pass through the prism while redirecting the acoustic waves at 90 degrees. (a) The first reflector experiment used a 25 mm right angle prism. (b) A parallel prism reflector, with better spectral performance, made up of four 6 mm by 16 mm prisms (outlined in red) bonded together to produce a trapezoidal profile (outlined in green).

2.3 Photoacoustic Enabling Device (PED)

After experimenting with the acoustic reflectors mentioned in Section 2.2, we built a prototype of the PA attachment using a microscope slide. The fundamental feature of the PED, allowing the system to be practical, is the reflector chamber. Figure 3 shows a zoomed-in view of the reflector chamber with respect to the transducer. This chamber contains water and an optically transparent acoustic reflector mounted at an angle. We mounted the reflector at 45 degrees with respect to the transducer in order to obtain near 100% theoretical acoustic reflection as shown previously¹⁵. The wall of the chamber facing the back of the reflector contains a glass window to allow light to enter, while still maintaining a rigid sealed structure. The wall opposite this contains an acoustic window lined with a thin membrane (3MTM TegadermTM).

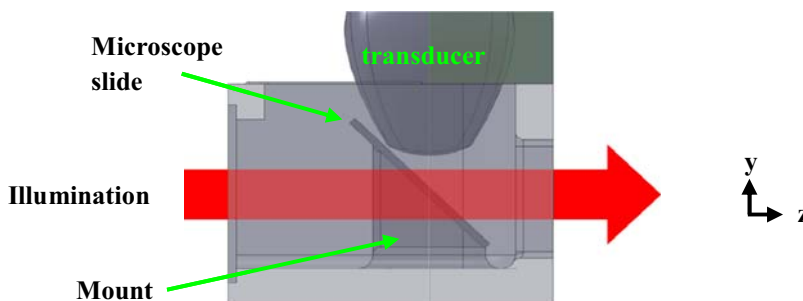


Figure 3. A zoomed-in view of the actual computer-aided design (SolidWorksTM) used to manufacture the reflector chamber. The walls of the chamber are shown semi-transparent to enable viewing of the reflecting glass inside. This chamber would normally be filled with diH₂O.

The body of the device was designed in SolidWorks® and printed with an Objet Connex500™ using Objet FullCure®720 into a transparent acrylic based form. The transducer attaches to the device using a form-fitting mold that locks the position of the transducer. Our first design builds the reflector chamber directly attached to the mount for a “set and forget” style that ensures a constant geometric positioning between the reflector and the face of the transducer. Figure 4 shows photographs of the finished product by itself and with the ultrasound probe mounted. This study applied free space illumination through the PED, while we continue to develop the illumination block for future iterations of the device.



Figure 4. (Left) Two halves of the PED are shown unattached to a clinical probe. A microscope slide serves as the acoustic reflector inside the optical chamber. (Right) The PED mounted to a 10 MHz clinical scanner (Zonare Medical Systems). The acoustic window at the face is made out of 3M™ Tegaderm™. Acoustic coupling to tissue can be achieved by applying acoustic coupling gel, similar to a typical PE examination.

2.4 Experimental Setup

The experimental setup to demonstrate the feasibility of the PED used imaging equipment described previously for real-time simultaneous PE and PAI¹². The source of light is a frequency doubled Q-switched Nd:YAG laser (Continuum Surelite™ I-20) pumping an optical parametric oscillator (Continuum Surelite™ OPO PLUS) to provide laser pulses at selectable wavelengths between 680 nm and 2000 nm. Experiments on phantoms were conducted with the laser output set to 700 nm and synchronized with a clinical ultrasound scanner (z.one *ultra*, Zonare Medical Systems) using a field-programmable gate array (FPGA). Zonare’s L10-5 linear array transducer (7 MHz center frequency) contains 128 detector elements from which we can collect 64 channels simultaneously. Laser pulses (5 ns) were directed towards the phantom but passed through a diffuser centimeters before arriving at the object of interest. Measured fluences were 7 - 15 mJ/cm², within the energy density standards set by ANSI¹⁷. Matlab™ was used to control all instruments, manage the data collection and process the images. Figure 5 shows photos of some of the equipment with a schematic illustrating the setup and control flow.

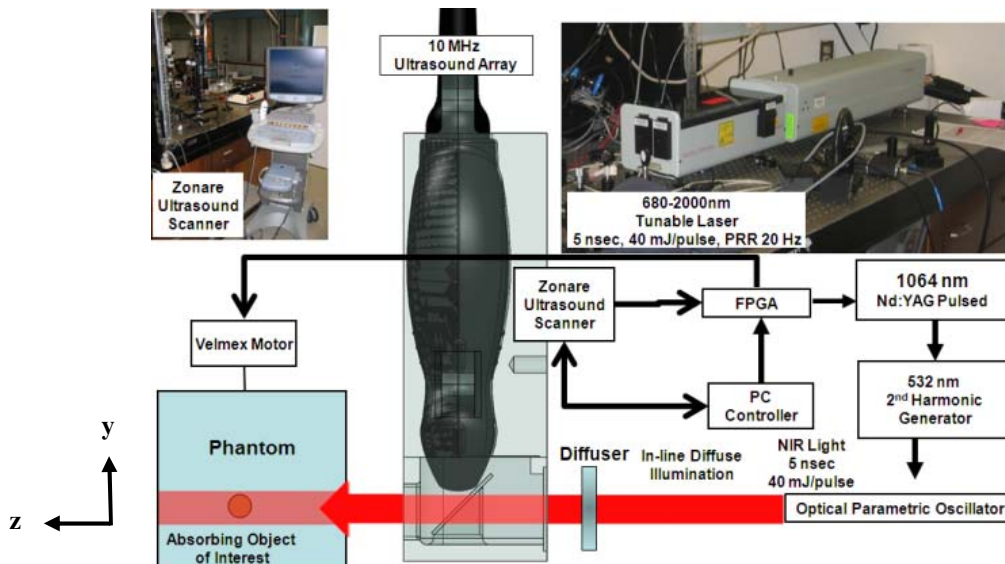


Figure 5. The experimental setup, hardware used, and the communication connections between them.

A motor (Velmex) moved the phantom linearly to collect three-dimensional (3D) data sets. Although this example does not illustrate the handheld capability of the PED, it does collect 3D data for side-by-side comparison to data collected without the PED. In the results presented, the phantom was scanned at a rate of 1 mm/s acquiring 20 fps for an inter-frame distance of 50 μm . The PA data acquisition rate is limited by the pulse repetition rate of the laser set to 20 Hz.

2.5 Phantoms

Various simple phantoms were scanned and imaged in order to validate that the imaging properties of the system were performing as expected. Early experiments used simple phantoms such as crossing strings, a graphite rod, a taught thread and a rat tail. The purpose of these experiments was to compare our PED results with conventional scanning (no PED) and to visually confirm the accuracy of the images.

Using the final PED, PA and PE data were acquired simultaneously of a stationary wire target and for a transparency with a printed image. PA images and PE images were formed delay and sum beamforming based on one way and two way propagation, respectively. A thin wire ($d=127\ \mu\text{m}$) allowed us to calibrate the laser firing with respect to the initial acoustic plane wave excitation. When the beam forming timing is close enough, the PE and PA images of the wire cross section will overlap. Figure 6 shows photographs of the transparency phantom and setup.

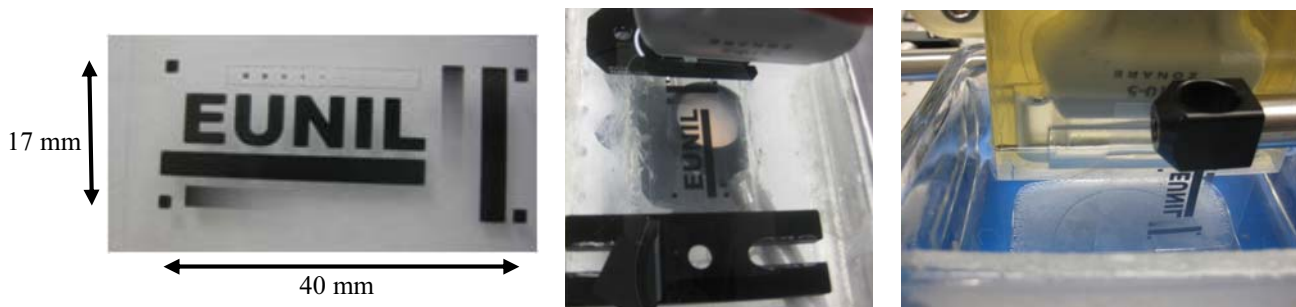


Figure 6. (Left) Photograph of a design laser-printed on a transparency used as a test phantom for comparison. (Middle) Conventional transillumination phantom scan in a water tank. (Right) Setup used to scan the phantom, with reflection-mode illumination, using the PED. In future studies, the probe can be held freehand with gel coupling to the skin.

3. RESULTS AND DISCUSSION

3.1 Early Prototype In-Line Reflectors

The resulting images of the rod phantom using the 25 mm right angle prism (see Fig. 2a) were encouraging. The images of the rod using this reflector show minimal image degradation (Figure 7). The size of the rod of the rod was 0.40 mm (lateral) by 0.50 mm (axial) [FWHM].

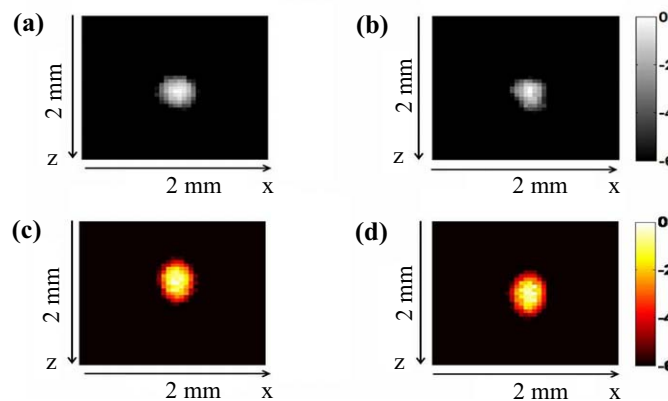


Figure 7. Images of a 0.5 mm graphite rod with no lateral smoothing. (a) PE image without the reflector. (b) PE image with the reflector. (c) PA image without the reflector and using 680 nm light. (d) PA image with the reflector and using 680 nm light.

Applying the bonded-prisms reflector on a thread longitudinally gives a better indicator of the real-time image acquisition of this test (Figure 8). In the PE image, the structure of the thread is clear while the PAI, at 700 nm, shows two vertical shadows around the lateral 8 mm mark. The shadow can be explained by the slightly convex beveled edge of each prism focusing more light to their respective centers causing a lack of optical fluence on the edge of the prism.

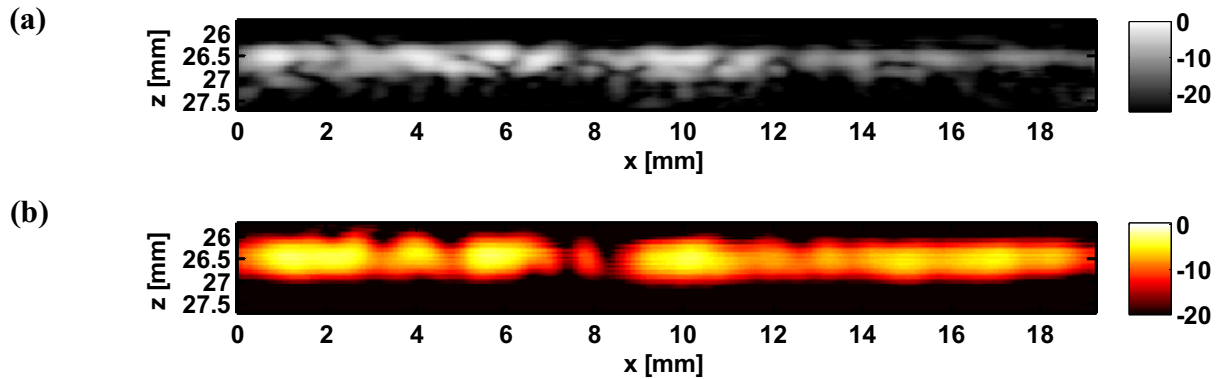


Figure 8. Longitudinal image of a thread using bonded prisms as the reflector (see Figure 2b). (a) A real-time PE image, mapping surface features of the thread diameter. (b) A real-time acquisition PA image mapping the illumination with 700 nm light upon the thread. The artifact at 8 mm might be due to the small curved surface on the bottom edge of each prism, which effectively deflects light away from this region.

The images of a tail from a fresh rat cadaver, in Figure 9, demonstrate how we might use the device to image a small animal. The PE image delineates the surface boundaries of the tail and illustrates that the diameter is approximately 5 mm long. In the PA image using 700 nm light, it can be seen that most of the light is absorbed in the first 2 mm of the tail. Absorption in the tail might be from clotted blood. These results demonstrate the capabilities for the PED to image biological tissue, which can include applications for breast cancer, but also incorporate small animal biomedical research, such as monitoring prostate tumor growth in a mouse model¹⁸.

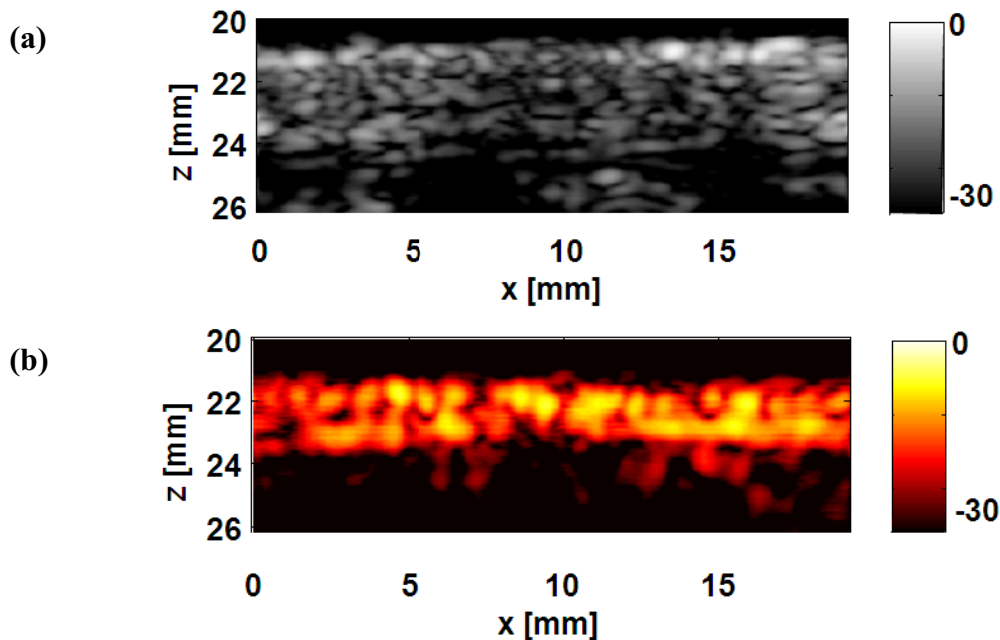


Figure 9. A longitudinal image of a rat tail using the bonded-prisms reflector to demonstrate an application on biological tissue. (a) Real-time acquisition PE image outlining the diameter of the tail about 5 mm. (b) Simultaneously acquired real-time acquisition PA image showing that 700 nm light can penetrate the tail at least 2 mm. Scale bars are in dB.

3.2 Photoacoustic Enabling Device: Dual Modality Accuracy

After experimenting with different designs for the essential acoustic reflector, the chosen reflector, a microscope slide, was integrated into a simple and compact attachment to a clinical ultrasound machine. Using this final design, the images shown in Figure 10 demonstrate the close co-registration of the PE data with the PA data. These figures are plotted on exactly the same scales and in both cases, the wire is found at the same imaging depth, about 25 mm from the probe surface. The images on the left (Figure 10, left), shows features down to -35 dB where the beam forming artifacts can be seen. In addition, noise can be seen in the PA image down to -35 dB giving us a feel for the noise level of the PA setup. The images on the right of Figure 10 are plotted so that signals above the FWHM are shown. The symmetrical characteristic of these images illustrate the accurate imaging capability of the PED. The resolution in the axial dimension between the PA and PE images are different due to the one way versus two way propagation.

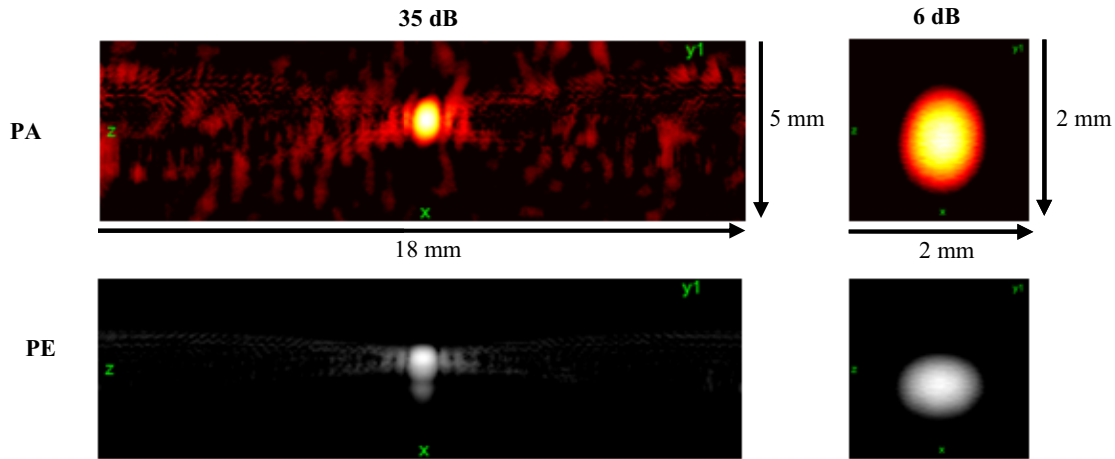


Figure 10. Images of the cross section of a 127 μm Teflon blue wire with no averaging. The two images on the left are both shown with a 25 dB hot color scale. The two images on the right are both shown with 6 dB hot color scales on the same axis (both depth and laterally) to show the close agreement between the axial positions.

3.3 Comparison of PED with the Conventional Method

The transparency phantom (Figure 6) was imaged using conventional techniques and using the PED attached to the same US probe. However, since the transparency is thin and not rigorously aligned, the entire plane of the transparency does not appear at a single imaging depth. Therefore, to compare the images using the two methods, we calculated the maximum amplitude projection (MAP) of the 3D dataset (Figure 11). Moreover, to illustrate the 3D aspect of the phantom we show a 3D rendering of the same data using our PED in Figure 12.

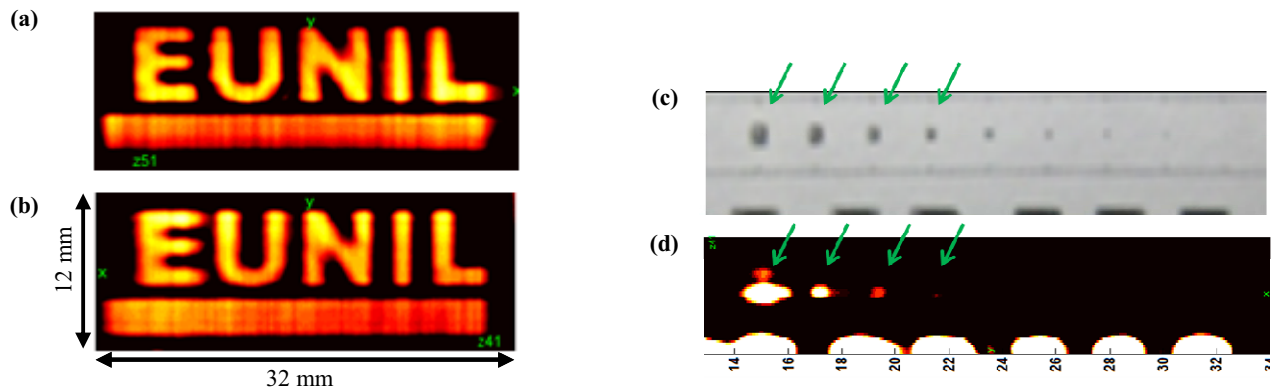


Figure 11. Maximum projection along the axial (z) directions of the scanned phantom. Both images are plotted on a -15 dB hot scale from the maximum with similar dimensions. Images were acquired using 700 nm light with approximately 12 mJ/cm^2 of fluence. The image shown in (a) was produced with data acquired using conventional imaging methods of a phantom in water with transillumination. The image in (b) was produced from data acquired

using our PED. (c) and (d) show a photograph and a -18 dB PA image, respectively, of similar regions. The dimensions of the first four squares (pointed by green arrows) in the images are 550, 466, 381 and 296 μm square.

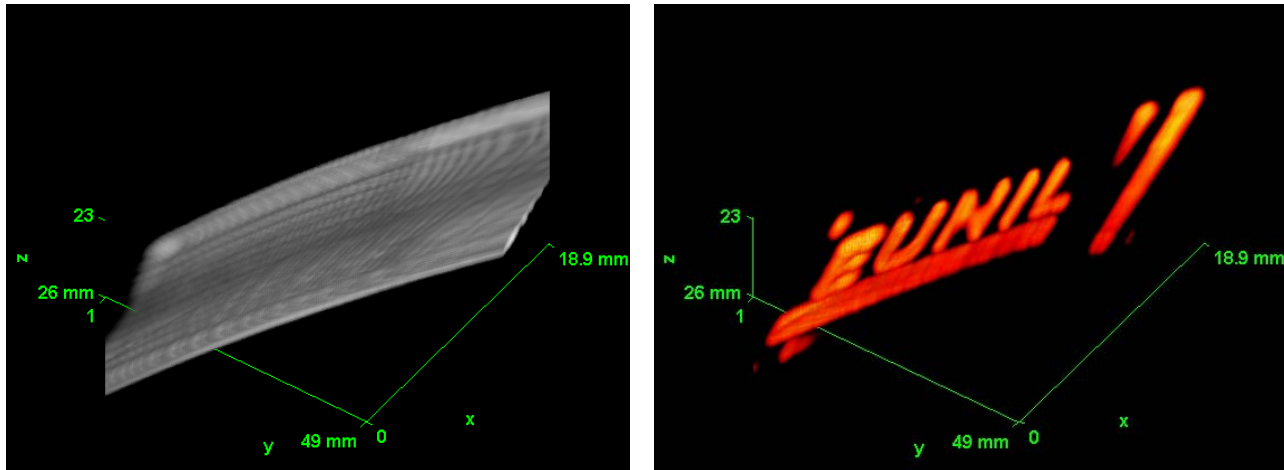


Figure 12. (Left) 3D rendering of the PE image of the transparency phantom. (Right) 3D rendering of the PA data of the same transparency at the same angle as the PE image. This demonstrates the 3D imaging capabilities of the real-time dual-modality imaging system made possible by the PED.

The MAP images, shown in Figure 11, confirm that the use of the PED does not introduce appreciable distortions and is comparable to the use of the transducer without the reflector. Furthermore, the PED enables on-axis illumination in reflection mode independent of wavelength. The PED also makes PA imaging more practical for medical applications since it uses handheld methods common with clinical ultrasound, except that the probe must be angled at 90 degrees during a freehand scan. Differences between the two “EUNIL” images can largely be attributed to differences in the illumination pattern for the two different setups. Interestingly, at a scale of -18 dB from the maximum, one can already see the first four squares printed on the phantom. The dimensions of these four squares are 550, 466, 381 and 296 μm square from left to right. One can also see clearly confirm their position relative to the top edge of the letters in both the photograph and the PAI.

The current prototype can be used to further study and characterize the system for tissue imaging. However, many alterations must be implemented before the device can be used in a clinical setting. Modifying the illumination portion of the design to be fiber coupled to a compact and portable source will make this system truly mobile. Second, the mold and form of the current prototype should be minimized in size for clinicians to find ergonomically comfortable. Incorporating these improvements and studying the images in conjunction with contrast agents would further research in cardiac and neuroimaging^{5, 18-21}.

4. CONCLUSION

This study demonstrated the development and testing of an attachment to a clinical ultrasound probe enabling real-time PE and PAI. The PED circumvents current illumination challenges by allowing wavelength independent direct illumination. Images of wire and a transparency image qualitatively suggest the system works. The design is practical, inexpensive and compatible with current clinical ultrasound systems. The PED can be readily adapted for breast imaging and would facilitate clinical trials for detecting cancer using a dual-modality PA and PE freehand imaging system.

ACKNOWLEDGEMENTS

This work was supported in part by grants from the National Science Foundation (NSF-0853618), the Technology and Research Initiative (TRIF), the Advanced Research Institute for Biomedical Imaging (ARIBI), AZCC Seed Grant (IRG-7400128) and with support from Zonare Medical Systems.

REFERENCES

- [1] Parkin, D. M., Bray, F., Ferlay, J. and Pisani, P., "Global Cancer Statistics, 2002," *C. A. Cancer J. Clin.* 55, 74-108 (2005).
- [2] Smith, J. A. and Anddrepoulou, E., "An overview of the status of imaging screening technology for breast cancer." *Ann. Oncol.* 15, 118-126 (2004).
- [3] Manohar, S., Vaartjes, S. E., van Hespén, J. C. G., Klasse, J. M., van den Engh, F. M., Steenbergen, W. and van Leeuwen, T. G., "Initial results of *in vivo* non-invasive cancer imaging in the human breast using near-infrared photoacoustics," *Optics Express* 15(19), 1227-12285 (2007)
- [4] Ermilov, S. A., Khamapirad, T., Conjusteau, A., Leonard, M. H., Lacewell, R., Mehta, K., Miller, T. and Oraevsky, A. A., "Laser optoacoustic imaging system for detection of breast cancer," *Journal of Biomedical Optics* 14(2), 024007 (2009).
- [5] Olafsson, R., Montilla, L. G., Ingram, P. and Witte, R. S., "Tracking contrast agents using real-time 2D photoacoustic imaging system for cardiac applications," *Proc. SPIE* 7177, 71771R (2009).
- [6] Park, S., Mallidi, S., Karpiouk, A. B., Aglyamov, S. and Emelianov, S. Y., "Photoacoustic Imaging Using Array Transducer," *Proc. SPIE* 6437, 643714 (2007).
- [7] Emelianov, S. Y., Aglyamov, S. R., Shah, J., Sethuraman, S., Scott, W. G., Schmitt, R., Motamedi, M., Karpiouk, A. and Oraevsky, A., "Combined ultrasound, optoacoustic and elastic imaging," *Proc. SPIE* 5320, 101-112 (2004).
- [8] Zhang, H.F., Maslov, K., Stoica, G. and Wang, L. V., "Functional photoacoustic microscopy for high-resolution and noninvasive *in vivo* imaging." *Nature Biotechnology* 24, 848-851 (2006).
- [9] Shan, Q., Dewhurst, R.J., Kuhn, A., Pang, K.F. and Payne, P.A., "Modelling of a photoacoustic probe designed for medical applications," *Ultrasonics* 34, 575-577 (1996).
- [10] Maslov, K., Stoica, G. and Wang, L. V., "*In vivo* dark-field reflection-mode photoacoustic microscopy," *Optics Letters* 30(6), 625-627 (2005).
- [11] Maslov, K. Zhang, H. F., Hu, S. and Wang, L. V., "Optical-resolution photoacoustic microscopy for *in vivo* imaging of single capillaries," *Optics Letters* 33(9), 929-931(2008).
- [12] Niederhauser, J.J., Jaeger, M., Hejazi, M., Keppner, H. and Frenz, M., "Transparent ITO coated PVDF transducer for optoacoustic depth profiling," *Optics Communications* 253, 401-406 (2005).
- [13] Manohar, S., Kharine, A., van Hespén, J. C. G., Steenbergen, W. and van Leeuwen, T. G., "The Twente Photoacoustic Mammoscope: system overview and performance," *Phys. Med. Biol.* 50, 2543-2557 (2005).
- [14] Oraevsky, A. A., Karabutov, A. A., Solomatin, S. V., Savateeva, E. A., Andreev, V. G., Gatalica, Z., Singh, H. and Fleming, D. R., "Laser optoacoustic imaging of breast cancer *in vivo*," *Proc. SPIE* 4256, 6-15 (2001).
- [15] Zemp, R. J., Ranasinghesagara, J., Jiang, Y., Xuhui, C. and Mathewson, K., "A Photoacoustic Method for Optical Scattering Measurements in Turbid Media," *Proc. SPIE* 7177, 71770Q (2009).
- [16] Montilla, L. G., Witte, R. S., Olafsson, R., "Method and Apparatus for In-Line Photoacoustic Imaging," U.S. provisional patent 10062, (2010).
- [17] A. N. S. Institute, "American National Standard for the Safe Use of Lasers," American National Standards Institute, (2000).
- [18] Bauer, D. R., Olafsson, R., Montilla, L. G. and Witte, R. S., "*In vivo* multi-modality photoacoustic tracking of prostate tumor growth using a window chamber," *Proc. SPIE* 7564, "in press" (2010).
- [19] Witte, R. S., Huang, S., Ashkenazi, S., Kim, K. and O'Donnell, M., "Contrast-enhanced photoacoustic imaging of live lobster nerve cord," *Proc. SPIE* 6437, 64370J (2007).
- [20] Witte, R. S., Kim, K., Ashish, A., Kopelman, R., Kotov, N., Kipke, D. and O'Donnell, M., "Enhanced photoacoustic neuroimaging with gold nanorods and PEBBLEs," *Proc. SPIE* 685614, 685614-1 (2008).
- [21] Kim, K., Agarwal, A., Mcdonald, A.M., Moore, R.M., Myers, D.D., Witte, R.S., Huang, S.-W., Ashkenazi, S., Kaplan, M.J., Wakefield, T.W., O'Donnell, M. and Kotov, N.A., "*In vivo* imaging of inflammatory responses by photoacoustics using cell-targeted gold nanorods (GNR) as contrast agent," *Proc. SPIE* 68560, 68560H (2008).